Structural Metamaterials with Saint-Venant Edge Effect Reversal

Eduard G. Karpov

Civil & Materials Engineering, University of Illinois at Chicago,

842 W Taylor St, Chicago, IL 60607. Email: ekarpov@uic.edu

Abstract

When a usual material is loaded statically at surfaces, fine fluctuations of surface strain diminish fast in the material volume with the distance to the surface, a phenomenon widely known as the Saint-Venant edge effect. In this paper, highly nonlocal discrete lattices are explored to demonstrate structural metamaterials featuring *reversal* of the Saint-Venant edge effect. In these materials, certain coarse patterns of surface strain may decay faster than the finer ones. This phenomenon is shown to arise from anomalous behavior of the Fourier modes of static deformation in the material, and creates opportunities for blockage, qualitative modification and in-situ recognition of surface load patterns. Potential applications and useful practical techniques of spectral analysis of deformation, density of states and phase diagram mapping are outlined.

Keywords: mechanical metamaterial; Saint-Venant edge effect; Fourier methods

1. Introduction

The notion of metamaterials refers to an exciting class of man-made material systems with engineered internal structure (embedded resonators, elastic links, metastable elements, etc.) leading to a negative or reverse effective material property. Such a property usually occurs due to a nontrivial collective behavior of many individual structural elements functioning in a synergistic manner. While basic properties of those individual elements can be simple (linear), the interesting collective behavior is owed to a cooperation between the elements achieved with a proper design of their internal structure and interactions. Generally, photonic/electromagnetic, phononic/acoustic and mechanical metamaterials are distinguished [1-34].

1

Photonic metamaterials are the earliest known class of metamaterials, where the negative effective electrical permittivity (ε) and electromagnetic permeability (μ) are attained simultaneously at the expense of a microscopic superlattice resonator structure leading to a dispersive, nonlinear photonic spectrum. A negative refractive index and the absence of light reflection at an interface of a metamaterial with $\varepsilon < 0$ and $\mu < 0$ and a usual media was first predicted in a 1968 publication [1]. These basic phenomena, in turn, imply amazing practical opportunities, such as superlense and "invisibility cloak" applications [1-7]. One more recent class of photonic metamaterials are plasmonic systems [8-14] featuring nonlinear spectra of collective electron excitation frequencies. Such spectra can provide an efficient generation of higher frequency harmonics, and geometrical and spectral localization of the incident photon energy, being key phenomena for the enhanced photovoltaics, photocatalytic water splitting and other applications [8-14].

Phononic and acoustic metamaterials are dynamical material systems with simple constitutive properties of the individual elements, but counterintuitive collective properties, such as the negative effective mass density and others [15-27]. These unusual collective properties can be realized from the nonlinear vibration frequency spectra, or dispersion relationships $\omega(\mathbf{k})$, where $\mathbf{k}$ is the Fourier wave vector, obtained by applying Fourier transform in time and space to a structural or multi-body dynamics equation. Opportunities for very interesting phenomena, such as acoustic shielding and cloaking arise from the gaps between distinct dispersion branches $\omega_i(\mathbf{k})$, leading to a wide range of important applications ranging from sound insulation and vibration energy harvesting to nondestructive testing and earthquake engineering.

Structural & mechanical metamaterials [28-34,46-48] show *quasistatic* responses to loads that can be interpreted as a negative effective elastic modulus or a negative Poisson ratio by a combination of simple microstructural elements, bars and springs. One recent development [31-34], including by this author and a co-worker [33-34], also uses a structural bistability at the unit cell level that could deploy a polymorphic type phase transformation in the entire material. If properly designed, such a phase transformation can lead to a contraction of the material in the direction of an increasing external load, the negative extensibility phenomenon. Origami structures provide another interesting type of mechanical metamaterials [46-48] where negative Poisson's ratio, bending and twisting stiffness are either analytically expressed or numerically observed. The work by Silverberg and co-workers [48] is also an example of using bistability of a unit cell to fold reprogrammable mechanical metamaterials based on origami structures.

In this paper, we provide a mathematical foundation and demonstrate the paths toward design and fabrication of a class of structural metamaterials featuring a Reverse Saint-Venant (RSV) edge effect, or shorter the *RSV metamaterials.* When a usual material or structure is loaded statically at surfaces, fine fluctuations of surface strain diminish fast in the material or structure interior with distance to the surface, a phenomenon widely known as the Saint-Venant edge effect, e.g. [35-36]. In this paper, we have explored some discrete lattices with a higher degree of nonlocality as possible engineered base structures of the RSV metamaterials. In these lattices, certain *coarse* patterns of surface strain may decay faster than the finer ones. More remarkably, such materials will be shown to have an ability to completely block or qualitatively modify certain types of static deformation at surfaces.

The Saint-Venant edge effect is perceived so naturally that one could hardly imagine any violations of it in a material system. Nonetheless, in Section 2, we provide a rigorous proof of concept, followed by discussions of interesting practical opportunities in Section 3, including surface arrest of static deformation and qualitative modification of strain and stress patterns. Conclusions are given in Sections 4. Practical opprtunities of the RSV metamaterials are discussed in the context of the density of states calculation, spectral analysis of deformation and phase daigram mapping.

2. Fourier Modes of Free Static Deformation

We generally suggest that the Saint-Venant edge effect reversal may occur in materials with internal micro- or mesostructure featuring *nonlocal* interactions. Analysis of these interactions and the resultant effective material properties requires a discrete nonlocal elastic formulation.

Below in this section we suggest a formulation leading directly to the desired metamaterial behavior in a simple but rigorous manner. First we will show that in a local isotropic elastic continuum, only the usual Saint-Venant behavior is possible, and the nonlocality has to be a necessary condition for the sought behavior.

For this discussion, it will be convenient to introduce a nonstandard property of an elastic medium or lattice that we may call the Fourier spectrum of deformation decay parameters, or shorter, *deformation decay spectrum*. This spectrum is a key element of the analytical method offered here, and it exists for any local or nonlocal continuum or a discontinuous structure. In the further discussion (Sections 2.2-2.5) we will see that the Saint-Venant edge effect reversal and surface load

arrest phenomena would require occurrence of *asymptotic bandgaps* in the spectrum. In turn, such bandgaps will imply nonlinear and non-monotonous spectral behaviors, only possible in nonlocal media. This spectrum is somewhat analogous, but not similar to the acoustic wave frequency spectrum of a dynamical structure [15-27], where the bandgaps can lead to an acoustic metamaterial.

2.1 Deformation decay spectrum of a continuum solid

Consider a state of plain strain in a *continuum half-plane* for boundary conditions $u(0,y)$ and $v(0,y)$, governed by the homogenous Navier's equations [37] over $x > 0$,

$$2(1-v)\frac{\partial^2 u}{\partial x^2} + \frac{\partial^2 v}{\partial x \partial y} + (1-2v)\frac{\partial^2 u}{\partial y^2} = 0,$$

$$(1-2v)\frac{\partial^2 v}{\partial x^2} + \frac{\partial^2 u}{\partial x \partial y} + 2(1-v)\frac{\partial^2 v}{\partial y^2} = 0$$

$$(1)$$

Since any deformation must disappear when $x \to \infty$, it is interesting to consider a fundamental solution as a *decaying Fourier mode* of free static deformation (at real positive η and complex C_i):

$$u(x,y) = C_1 e^{-\eta x} e^{iqy}, \quad v(x,y) = C_2 e^{-\eta x} e^{iqy}, \quad q \in (-\pi, \pi) \tag{2}$$

Here, q is a Fourier parameter of the mode. When necessary, two independent real-valued solutions can be constructed by taking separately the real and imaginary parts of (2).

Substituting (2) into the governing equation (1) gives two characteristic equations,

$$2\eta^2(v-1)C_1 + iq\eta C_2 - q^2(2v-1)C_1 = 0,$$

$$\eta^2(1-2v)C_2 - iq\eta C_1 + 2q^2(v-1)C_2 = 0 \tag{3}$$

These equations indicate that (2) can be a true solution, indeed, but only if $\eta = \pm q$ and $C_2 = \mp iC_1$. A solution satisfying specific boundary conditions can be obtained as a superposition of the modes (2) with the amplitudes determined by standard Fourier methods. The value η should remain positive for any q, and therefore, we can write

$$\eta(q) = |q| \tag{4}$$

This relationship between the decay parameter and the Fourier parameter, Fig.1, represents the simplest *deformation decay spectrum* of an elastic medium or structure. It applies to any homogenous and isotropic material governed by (1). We will also call such a relationship the "η-distribution" below. It will become more sophisticated in the analysis of discrete lattices.

Physical meaning of the decaying mode solution (2,4) can be illustrated as follows. Assume there is a surface traction at $x = 0$ leading to the boundary displacements,

$$u(0, y) = a\cos(q \cdot y), \quad v(0, y) = a\sin(q \cdot y) \tag{5}$$

Then, the real amplitude a of these displacements will diminish at $x > 0$ with the factor $e^{-|q|x}$, and all strain and stress components will decrease with the same factor as well. Thus, the value $\eta = |q|$ can be interpreted as a basic exponential *decay parameter* of the corresponding Fourier mode of static deformation occurring at the boundary.

For the discussion to follow, we note that Fig.1 spectrum is naturally consistent with the usual *Saint-Venant edge effect*: Fourier modes corresponding to higher values q (having shorter distances between two nearest maxima or minima) decay faster with x; see Fig.2.

2.2 Deformation decay spectrum of a discrete lattice

Consider a periodic elastic system, naturally discrete or discretized one, which can be a network of elastic elements or a continuous matrix with internal structure (voids, inclusions, etc.), where some important *nodal* degrees of freedom can be introduced. Assume that a repeating node or a set of repeating nodes (n,m) may interact directly with some neighbor sets (n',m'); see examples in Figs.3-4 and also Fig.6. The mechanical response of this material to an external load at (n,m) will depend on the state of deformation not only at (n,m), but also in a *finite region* encompassing all the nodes (n',m'). This latter fact is a manifest of the nonlocal nature of the discrete or structured material systems. As we will see below, certain farer reaching interactions being sufficiently strong may lead to dramatic changes of the basic mechanical properties, including qualitative changes in the deformation decay spectrum. In particular, some systems may show regions with *negative* decay factors equivalent to $e^{-\eta}$ in the continuum solution (2), requiring a complex η. Physical meaning and practical importance of the complex η are discussed below in Sections 2.4-2.5.

The deformation decay spectrum of a periodic lattice or structure with only nodal degrees of freedom can be analyzed as the following. We assume a 2D periodicity, where two integer indices (n,m) can define a repeating node or set of nodes, and a 3D extension is straightforward. We introduce an *associate substructure* of the material to include a current node (n,m) and all other nodes (n',m') interacting directly with (n,m), and write a *governing equation of equilibrium* of the nodes (n,m) using a discrete convolution ($*$) operator with a stiffness kernel **k**,

$$\left(\mathbf{k} * \mathbf{u}\right)_{n\,m} = \sum_{n'=n-\alpha}^{n+\alpha} \sum_{m'=m-\beta}^{m+\beta} \mathbf{k}_{n-n'\,m-m'}\,\mathbf{u}_{n'\,m'} = \mathbf{f}_{n\,m}, \quad n = 0, \pm 1, ..., \quad m = 0, \pm 1, ... \quad (6)$$

Here, $\mathbf{u}_{nm}$ and $\mathbf{f}_{nm}$ are vectors of displacements/rotations and external forces/moments at (n,m), respectively; the summations run over all the neighbor nodes (n',m') in the associate cell; and $\mathbf{k}$ are small matrices that describe the intensity of all possible elastic interactions of the node (n,m) with its neighbors [38-39]. The $\mathbf{k}$-matrices can be obtained in practice as respective blocks of some bar, beam or solid element stiffness matrices, similar to those used in the finite element analysis. The associate cell is a minimal part of the periodic structure that fully represents its mechanical properties [38-45].

Assume that the material is loaded at nodes with $n = 0$ only, and an essential boundary condition $\mathbf{u}_{0,m}$ is known. For a compact discussion, we take $\alpha = 1$ in (6), and a more general case can be studied similarly by increasing the set (n,m). Then, for the $n > 0$ half-plane, equation (6) becomes

$$\sum_{m'=m-\beta}^{m+\beta} \left(\mathbf{k}_{1\,m-m'}\,\mathbf{u}_{n-1\,m'} + \mathbf{k}_{0\,m-m'}\,\mathbf{u}_{n\,m'} + \mathbf{k}_{-1\,m-m'}\,\mathbf{u}_{n+1\,m'} \right) = \mathbf{0} \qquad (n > 0) \qquad (7)$$

By analogy with (2), we will study a fundamental solution for (7) as *decaying Fourier mode* of free static deformation

$$\mathbf{u}_{n\,m} = C\mathbf{h}(q)e^{-\eta(q)n}\,e^{iqm}, \qquad q \in (-\pi, \pi) \qquad (8)$$

Here, C is an amplitude, $\mathbf{h}$ is a normalized deformation *"mode shape"* vector, the *decay parameter η* is analogous to that in (2), and q can take discrete values if the lattice is finite along m.

Apply the discrete Fourier transform in space over index m in (8) and use the shift and convolution theorems (A1-A3) to get a simple algebraic form of the equation (7) in the Fourier domain,

$$\mathbf{K}_1(q)\mathbf{U}_{n-1}(q) + \mathbf{K}_0(q)\mathbf{U}_n(q) + \mathbf{K}_{-1}(q)\mathbf{U}_{n+1}(q) = \mathbf{0}, \qquad (9)$$

$$\mathbf{K}_n(q) = \sum_{m=-\beta}^{\beta} \mathbf{k}_{n\,m}e^{-iqm}, \quad \mathbf{U}_n(q) = a\mathbf{h}(q)e^{-\eta(q)n} \qquad (10)$$

Equation (9) can be rewritten in a recurrent form,

$$\begin{Bmatrix} \mathbf{U}_n(q) \\ \mathbf{U}_{n+1}(q) \end{Bmatrix} = \mathbf{H}(q)\begin{Bmatrix} \mathbf{U}_{n-1}(q) \\ \mathbf{U}_n(q) \end{Bmatrix}, \quad \mathbf{H}(q) = \begin{bmatrix} \mathbf{0} & \mathbf{I} \\ -\mathbf{K}_{-1}(q)^{-1}\mathbf{K}_1(q) & -\mathbf{K}_{-1}(q)^{-1}\mathbf{K}_0(q) \end{bmatrix} \qquad (11)$$

where **H** is a *q*-parametric *transfer matrix*. Importantly, eigenvectors of such a matrix must have a structure, where the bottom half-vector is equal to the top half-vector multiplied by the eigenvalue, and all the eigenvalues come in reciprocal pairs $\{\lambda, 1/\lambda\}$. Therefore, the Fourier domain solution (10) will satisfy (9), if $e^{-\eta}$ is equal to an eigenvalue λ of the transfer matrix **H** and **h** is the normalized half-eigenvector:

$$\mathbf{H}(q)\begin{Bmatrix} \mathbf{h}(q) \\ \lambda(q)\mathbf{h}(q) \end{Bmatrix} = \lambda(q)\begin{Bmatrix} \mathbf{h}(q) \\ \lambda(q)\mathbf{h}(q) \end{Bmatrix}, \qquad \lambda(q) = e^{-\eta(q)} \Leftrightarrow \begin{matrix} \mathrm{Re}\,\eta = -\log|\lambda|, \\ \mathrm{Im}\,\eta = -\arg\lambda \end{matrix} \qquad (12)$$

Also, the Fourier mode (8) will satisfy the space domain equation (7), and it can be further used to construct a real-valued Fourier series solution for any specific boundary condition $\mathbf{u}_{0,m}$.

A full set of values $\lambda(q)$ or $\eta(q)$ determined for all q will comprise an intrinsic λ- *or η-distribution branch* of the deformation decay spectrum. The matrix $\mathbf{H}(q)$ will give $2S$ such branches, where S is the number of DoF per nodes (n,m), and S physical branches (with $|\lambda| < 1$) can be selected.

Physical meaning of the solution (8) is similar to that of the continuous one (2,4). For example, a Fourier mode of the displacement field at $n = 0$ (*a* and **h** are real),

$$\mathbf{u}_{0m} = a\,\mathbf{h}(q)\cos(q\,m) \qquad (13)$$

will diminish at $n > 0$ with the factor $e^{-n(\mathrm{Re}\,\eta)}$. All the stress and strain components will decrease with same factor as well. Thus, the complex value η is a *generalized decay parameter* of the corresponding Fourier mode of free static deformation in the nonlocal medium (7). If the unit cell width is selected as a unit of length, Re η can be compared to the real-valued η in (2).

2.3 Example: Rectangular grid

The governing equation of equilibrium (7) for a rectangular grid of Fig.3 will include only five nonzero **k**-matrices. For a simple case of one DoF per node they become scalars. For example, if stiffnesses of elastic interactions for horizontal and vertical pairs of nodes respectively are κ_1 and κ_2, we may divide the entire equation (7) by κ_1, introduce a dimensionless $k = \kappa_2/\kappa_1$ and write

$$\begin{aligned} \mathbf{k}_{00} &= 2(1+k), \\ \mathbf{k}_{10} &= \mathbf{k}_{-10} = -1, \\ \mathbf{k}_{01} &= \mathbf{k}_{0-1} = -k \end{aligned} \qquad (14)$$

The parameter k describes relative stiffness of the vertical interactions with respect to the horizontal ones. The transfer matrix (11) and its physically significant eigenvalue ($|\lambda| < 1$ for all q) are:

$$\mathbf{H}(q) = \begin{pmatrix} 0 & 1 \\ -1 & 2 + 2k(1 - \cos q) \end{pmatrix} \tag{15}$$

$$\lambda(q) = 1 + k(1 - \cos q) - \sqrt{k(1 - \cos q)(2 + k(1 - \cos q))} \tag{16}$$

The λ-distribution (16) is positive for all q and k, and the corresponding η-distribution is *nonlinear*, see Fig.3, in contrast to the continuum case of Fig.1. This result gives an interesting analogy with the dynamical systems, where the frequency dispersion branches are linear for infinite continua and nonlinear for discrete periodic media [15-27]. On the other hand, the η-distribution of Fig.3 is *monotonous* for the entire range of q and any value k. Therefore, the *usual* Saint-Venant effect (Fig.2) is still valid for this grid, and no particularly interesting behavior can be expected here.

2.4 Example: X-braced lattice

Consider the X-braced latticework shown in Fig.4. If the diagonal members are not connected at their intersections to form a node, then this structure is a simple example of an *essentially nonlocal* system. Indeed, depending on stiffness of the diagonal links, displacements at (n,m) could lead to a greater force effect on a more distant node $(n+1,m+1)$, than on a nearer node $(n+1,m)$ or $(n,m+1)$.

For a compact discussion, we assume one (horizontal) DoF per node and write seven nonzero scalar stiffnesses for equation (7) in a dimensionless form,

$$\begin{aligned} \mathbf{k}_{00} &= 2 + 4k, \\ \mathbf{k}_{10} &= \mathbf{k}_{-10} = -1, \\ \mathbf{k}_{11} &= \mathbf{k}_{-1-1} = \mathbf{k}_{-11} = \mathbf{k}_{1-1} = -k \end{aligned} \tag{17}$$

Here, the parameter k gives a relative stiffness of the *diagonal* interactions with respect to the horizontal ones, and the vertical interactions are absent. The transfer matrix (11) becomes

$$\mathbf{H}(q) = \begin{pmatrix} 0 & 1 \\ -1 & \dfrac{2 + 4k}{1 + 2k \cos q} \end{pmatrix} \tag{18}$$

and its physics relevant eigenvalue ($|\lambda| < 1$ for all q) reads

$$\lambda(q) = \frac{1 + 2k \cos q}{1 + 2k + 2\sqrt{k(1 + k + k \cos q)(1 - \cos q)}} \tag{19}$$

Here, the root argument is positive for any q, i.e. this λ-distribution is real. The denominator is positive; however, the numerator can be negative at least for some q, provided that $k > 1/2$. This means that in systems with sufficiently strong nonlocal interactions, the λ-distribution can have a *negative region*, see Fig.4. This result is highly significant for the following reasons:

1) The decay factor $e^{-\eta} = \lambda$ in equation (8) is also negative, which is not possible for the usual continuum (1). This requires an *imaginary part* of η, according to (12).

2) Displacement directions of some Fourier modes (8) will be *inverted* at $\lambda < 0$ each time n goes from even to odd, or opposite.

3) Most importantly: a *zero eigenvalue* exists, when $k > 1/2$ and

$$q = \pm \arccos(-1/(2k)) \tag{20}$$

4) Thus, a boundary deformation pattern,

$$u_{0m} = a_1 \cos(qm) \tag{21}$$

   where a_1 is an arbitrary real number and q satisfies (20) will be blocked at $n = 0$ and will not propagate into the material interior at all.

5) Practically, a range of fast-decaying modes (21) can be identified in the vicinity of (20), where the eigenvalue (19) is very small. These modes can be used to reconstruct various deformation patterns decaying very close to the boundary.

6) According to (12), $\eta \to \infty$ when $\lambda \to 0$. Thus, sufficiently strong diagonal interactions in the X-braced lattice (17) lead to asymptotic *bandgaps* in its η-distribution, Fig.4. Positions of the *asymptotes* of these stopbands is defined by the equation (20).

7) Finally, a *reversal* of the Saint-Venant edge effect may occur due to the non-monotonous behavior of the η-distribution introduced by the stopbands (20): denser modes (21) may now propagate farer than sparser ones for a range of q, compare Figs.5 and 2. Indeed, by Fig.4 data (case $k = 3.0$), it is possible that $\eta(q_2) < \eta(q_1)$, even though $|q_2| > |q_1|$.

Thus, a discrete nonlocal medium (17) with Fig.4 internal structure can represent a *mechanical metamaterial* if the condition $k > 1/2$ holds. This metamaterial can have zero and negative decay

factors $e^{-\eta} = \lambda$, enabling *qualitative* modification or processing of static deformation patterns in space (blocking at surfaces, filtering and inversion). This provides further analogies with dynamical metamaterials, where the vibration frequencies become complex within a phonon stopband.

2.5. Farer nonlocalities

Consider a latticework where the nonlocal interactions extend further in the direction of index m, as depicted in Fig.6. For a lattice with one DoF per node, equation (7) will include eleven nonzero stiffnesses that can be written in a dimensionless form,

$$
\begin{aligned}
&\mathbf{k}_{00} = 2 + 4k^{(1)} + 4k^{(2)} \\
&\mathbf{k}_{10} = \mathbf{k}_{-10} = -1, \\
&\mathbf{k}_{11} = \mathbf{k}_{-1-1} = \mathbf{k}_{-11} = \mathbf{k}_{1-1} = -k^{(1)}, \\
&\mathbf{k}_{12} = \mathbf{k}_{-1-2} = \mathbf{k}_{-12} = \mathbf{k}_{1-2} = -k^{(2)}
\end{aligned}
\tag{22}
$$

Fig.6 shows the λ- and η-distributions for such a system, where $k^{(1)} = k^{(2)} \equiv k$. Interestingly, this system has *two distinct bandgaps* on each side of the λ-distribution. The maximum possible number of the bandgaps will generally characterize the order of nonlocality of an RSV metamaterial.

2.6. Multiple DoFs per node

Structures with S degrees of freedom per node will feature S different branches in their deformation decay spectrum by S physical eigenvalues, $|\lambda_i(q)| < 1$, and therefore S distinct branches in their λ- and η-distributions; examples are shown Fig.7. Bandgap availability in at least one of the branches indicate that certain deformation patterns determined by the corresponding value q and the mode shape vector $\mathbf{h}(q)$ in (8) can be blocked in such structures. In some cases, *complex* values λ may occur for a range of q. Then, the modulus $|\lambda|$ and argument $\arg \lambda$ will show, respectively, the decay and phase shift of the mode (8) along the coordinate n.

2.7. Numerical validation

A series of numerical experiments were performed to validate the Saint-Venant edge effect reversal and the deformation blockage capabilities in the lattices shown in Figs. 4 and 6, using a commercial FEM software package ANSYS. We constructed rectangular structures of various sizes,

$N \times M$ nodes, using linear elastic small-strain bar elements with only translation degrees of freedom and constrained vertical displacements of the nodes. Periodic boundary conditions were applied at the top ($m = N$) and bottom ($m = 0$) edges of the rectangular lattice as explained in [38] to provide a seamless cyclic model, topologically equivalent to a horizontally placed cylinder, where the effect of the top and bottom boundaries is absent. The entire right edge ($n = N$) of these lattice models was free standing in all cases. Various sinusoidal displacement profiles (21), with different wave numbers q were imposed as essential boundary conditions at the left edge ($n = 0$) of the lattices. Numerical solutions of problems with periodic boundary conditions were matching the 1DoF version of the analytical solution (8),

$$ u_{nm} = a_1 \cos(q\,m)\,e^{-\eta(q)n}, \qquad n = 1, 2, ..., N, \; m = 1, 2, ..., M \tag{23} $$

with an accuracy of 10^{-6} or better for sufficiently large N. When the parameter q was selected at the position of an asymptote in the η-distribution, where $\eta \to \infty$, the deformation was entirely constrained at the left edge ($n = 0$) of the models with periodic boundary conditions, and the displacements u_{nm} in the lattice interior ($n > 0$) were all zeros with at least 10^{-5} precision.

In summary to Section 2, we have shown that the nonlocal discrete materials can have negative values in their λ-distribution and asymptotic stopbands in the η-distribution, and therefore demonstrate the following *anomalies* in the behavior of the fundamental Fourier mode solution (8): (a) near-surface deformation arrest or blocking (Re $\eta \to \infty$) and filtering (large/small Re η), and (b) deformation pattern inversion (Im $\eta = \pi$) and phase shift (Im $\eta \neq 0$). These phenomena are accompanied by the Saint-Venant edge effect reversal, and they cannot occur in continuous materials or simpler lattice structures as one in Fig.3 and similar [49-50].

3. Overview of Practical Techniques and Applications

In this section, we discuss interesting practical opportunities for the unusual mechanical behavior of the RSV metamaterials, and outline some useful tools and techniques for accelerated analysis, property prediction, design and fabrication of these materials.

Potential applications of the RSV metamaterials can vary from mechanical actuators, crack growth arrest and pressure smoothing in foundation slabs, Fig.8(a), to deformation canceling in building trusses, aircraft fuselages and other aerospace applications. For example, it will be possible to

design a solid-state pressure sensor triggering a signal, only if a particular load type occurs on the material surface, Fig.8(b). This opens a broader possibility for smart material systems with embedded functions for autonomous load pattern processing and recognition, and decision making. Other applications include pressure alleviation, stress and strain shielding and bypassing using a cloaking layer of the metamaterial around a critical region.

On the other hand, design and fabrication of the RSV metamaterials requires understanding of their basic *bandgap engineering* principles, including general physical conditions in the lattice leading to multiple bandgaps and bandgap widening (slower approaching the asymptotes), and approaches to the q-value lowering for the asymptotes enabling coarser modes blockage. The tools and techniques outlined below can help to address practical design of the RSV metamaterials: density of states calculation, spectral analysis of deformation and phase diagram compilation.

3.1 Density of states

In the field of structural dynamics and phononic crystals [15-27], a wave propagation is a state, and it is insightful for the bandgap engineering to draw a frequency distribution of these states over the first Brillouin zone. Such a distribution is known as density of states (DOS), $P(\omega)$, and its physical meaning is the probability $P(\omega)d\omega$ for a naturally freely propagating wave to have a frequency in the range $\omega+d\omega$. By this analogy, we may introduce a *density of static states $P(\eta)$* showing a distribution of all potentially available Fourier modes (8), the states of free static deformation, versus their decay parameter η. Analysis of this distribution can provide further insight for the RSV metamaterial properties prediction and design.

One simple way to calculate the density of state $P(\eta)$ is the numerical histogram approach, where the Fourier parameter q is sampled in a step-wise manner over the interval $(-\pi, \pi)$, and the count numbers of the values $\eta(q)$ falling into different intervals of width $\Delta\eta$ are recorded. The sought numerical distribution $P(\eta)$ is then obtained by normalizing the histogram with the factor $N\Delta\eta$, where N is the total number of samples. Fig.9 shows an example of such a distribution evaluated for the X-braced lattice described in Fig.4 and Section 2.4. For the case of $k = 3.0$, corresponding to a metamaterial ($k > 1/2$), we logically see in Fig.9 a long tail of fast decaying states at larger Re η, i.e. the deformation blockage opportunity discussed earlier in Section 2. Furthermore, we also see a localized peak positioned at a small value, Re $\eta = 0.87$, implying existence of a large

number of *slow* decaying modes (8) with Re η around that value. A superposition of such modes on the surface ($n = 0$) will represent a deformation pattern that can propagate deeply into the material volume, and therefore a midrange "passband" peak on the $P(\eta)$ profile represents an opportunity for *in-situ recognition* of certain surface load patterns by observing abnormally large deformations in the material interior. Thus, behavior of the density of states function can be a general indicator of the available metamaterial capabilities.

3.2 Spectral Analysis of Deformation

One attractive feature of the RSV metamaterials is that the standard Fourier series procedures can be used to perform spectral analysis of the deformation [38-39,43-45]. Since every Fourier mode (8) is characterized by a decay parameter η, it is possible to analyze and predict the spatial modification and propagation depth of deformation patterns in the RSV metamaterials. In particular, one may determine how far a given surface pressure or deformation type can propagate and how its profile will change with a distance to the surface. An example of such analysis is shown in Fig.10. It is interesting to see that the RSV metamaterial, due to complex values η and resultant inversion and blockage of some of the modes (8), can disperse Gaussian deformation patterns, even though its constituent structural elements are linear. Such a nonlinear collective behavior is impossible for the elastic continuum (1) or even the usual lattice structures.

3.3 Phase diagrams and design guidelines

Outcomes of the analytical methods outlined earlier in this paper can be summarized in the form of phase diagrams enabling efficient design procedures and guidelines for the RSV metamaterials fabrication. The basic lattice structures, as shown Fig.4 and Fig.6 and others, can serve also as a reinforcement phase or skeleton for a softer continuous matrix to form a composite metamaterial with interesting resultant properties. Phase diagrams can be constructed in the design space of the composite or purely structural RSV metamaterials to show suitable combinations of parameters leading to the metamaterial behavior. Different possibilities, such as the decay and mode shape types, based on Re η, Im η and vector **h** components, and availability of single or multiple bandgaps can be additionally identified within the *metamaterial region* on these phase diagrams. An example of such a diagram for a purely structural material is shown in Fig.11.

4. Conclusions

When a usual material is loaded statically at surfaces, fine fluctuations of surface strain diminish fast in the material volume with distance to the surface, a phenomenon widely known as the Saint-Venant edge effect. In this paper, we have explored highly nonlocal discrete systems to demonstrate structural metamaterials featuring *reversal* of the Saint-Venant edge effect due to their specially designed internal structure. For these materials, certain coarse patterns of the surface strain may decay faster than the finer ones.

The concept of *deformation decay spectrum* (η-distribution) has been introduced on the basis of a transfer matrix eigenanalysis of a discrete lattice in the Fourier domain. Availability of *asymptotic bandgaps* in this distribution is an indicator that the metamaterial behavior is achievable for a given structural material. Mathematically, these bandgaps require a complex form and a nonlinear dependence of decay parameter η on the Fourier index q in the fundamental solution (8) of the governing equation (7). This contrasts the local continuum (1), where the η-distribution is linear and real, and even the usual discrete elastic media, where it can be nonlinear but remains real. A complex value η may lead to certain anomalous behaviors of the Fourier modes (8) of deformation in the metamaterial, including phase shift and inversion, and blockage at surfaces accompanied by the Saint-Venant edge effect reversal mentioned earlier.

These basic phenomena create opportunities for static deformation cloaking, filtering and inversion. More generally, they enable functional metamaterials for qualitative modification and recognition of static surface load patterns. Practical applications and techniques of the density of states, spectral analysis of deformation and phase diagram mapping have been outlined.

5. Acknowledgements

Appendix

Let x_m be a scalar, vector or matrix function of an integer parameter m. The *Discrete Fourier transform* of x_m is defined as a 2π-periodic function of a real-valued parameter p,

$$F_{m\to p}\{x_m\} = \sum_m x_m\, e^{-ipm} = X(p) \tag{A1}$$

where the *shift theorem* holds for any integer m',

$$F_{m\to p}\{x_{m+m'}\} = X(p)e^{ipm'} \tag{A2}$$

If y_m is another function of the parameter m, then the *convolution theorem* holds,

$$F_{m\to p}\{x*y\} = \sum_m \left(\sum_{m'} x_{m-m'}\, y_m \right) e^{-ipm} = X(p)Y(p) \tag{A3}$$

where $Y(p)$ is the discrete Fourier transform of y_m.

References

[1] Veselago VG. The Electrodynamics of Substances with Simultaneously Negative Values of ε and μ. *Sov. Phys. Uspekhi* 10(4), 509-514, 1968.

[2] Iwanaga M. Photonic Metamaterials: A New Class of Materials for Manipulating Light Waves, *Science and Technology of Advanced Materials* 13(5), 053002, 2012.

[3] Litchinitser NM, Shalaev VM. Photonic Metamaterials, *Laser Physics Letters* 5(6), 411-420, 2008.

[4] Jacob Z, Kim JY, Naik GV, Boltasseva A, Narimanov EE, Shalaev VM. Engineering Photonic Density of States using Metamaterials, *Applied Physics B Lasers and Optics* 100(1), 215-128, 2010.

[5] Ou JY, Plum E, Jiang L, Zheludev NI. Reconfigurable Photonic Metamaterials, *Nano Letters*, 11(5), 2142-2144, 2011.

[6] Khanikaev AB, Mousavi SH, Tse WK, Kargarian M, MacDonald AH, Shvets G. Photonic Topological Insulators, *Nature Materials* 12, 233-239, 2013.

[7] Soukoulis CM, Wegener M. Past Achievements and Future Challenges in the Development of Three-dimensional Photonic Metamaterials, *Nature Photonics* 5, 523-530, 2011.

[8] Atwater HA, Polman A. Plasmonics for Improved Photovoltaic Devices, *Nature Materials* 9, 205-2013, 2010.

[9] Morfa AJ, Rowlen KL, Reilly TH, Romero MJ, Lagemaat JVD. Plasmon-Enhanced Solar Energy Conversion in Organic Bulk Heterojunction Photovoltaics, *Applied Physics Letters* 92, 013504, 2008.

[10] Lindquist NC, Luhman WA, Oh SH, Holmes RJ. Plasmonic Nanocavity Arrays for Enhanced Efficiency in Organic Photovoltaic Cells, *Applied Physics Letters* 93, 123308, 2008.

[11] Hou W, Cronin SB. A Review of Surface Plasmon Resonance-Enhanced Photocatalysis, *Advanced Functional Materials* 23(13), 1612-1619, 2013.

[12] Lee J, Mubeen S, Ji X, Stucky GD, Moskovits M. Plasmonic Photoanodes for Solar Water Splitting with Visible Light, *Nano Letters* 12(9), 5014-5019, 2012.

[13] Linic S, Christopher P, Ingram DB. Plasmonic-Metal Nanostructures for Efficient Conversion of Solar to Chemical Energy, *Nature Materials* 10, 911-921, 2011.

[14] Zhang X, Chen YL, Liu RS, Tsai DP. Plasmonic Photocatalysis, *Reports On Progress In Physics* 76(4), 046401, 2013.

[15] Craster RV, Guenneau S (Eds.) *Acoustic Metamaterials: Negative Refraction, Imaging, Lensing and Cloaking*, Springer, 2013.

[16] Deymier PA (Ed.) *Acoustic Metamaterials and Phononic Crystals*, Springer, 2013.

[17] Zhou X, Liu X, Hu G. Elastic Metamaterials with Local Resonances: An Overview, *Theoretical and Applied Mechanics Letters* 2, 041001, 2012.

[18] Bilal OR, Hussein MI. Trampoline Metamaterial: Local Resonance Enhancement by Springboards, A*pplied Physics Letters* 103, 111901, 2013.

[19] Hussein MI, Leamy MJ, Ruzzene M. Dynamics of Phononic Materials and Structures: Historical Origins, Recent Progress, and Future Outlook. *Applied Mechanics Reviews* 66, 040802, 2014.

[20] Lin SCS, Huang TJ. Tunable Phononic Crystals with Anisotropic Inclusions, *Physical Review B* 83, 174303, 2011.

[21] Pichard H, Duclos A, Groby JP, Tournat V. Two-dimensional Discrete Granular Phononic Crystal for Shear Wave Control, *Physical Review B* 86, 134307, 2012

[22] Bilal OR, Hussein MI. Ultrawide Phononic Band Gap for Combined in-Plane and Out-of-Plane Waves. *Physical Review E* 84, 065701, 2011.

[23] Liu XN, Hu GK, Huang GL, Sun CT. An Elastic Metamaterial with Simultaneously Negative Mass Density and Bulk Modulus, *Applied Physics Letters* 98, 251907, 2011.

[24] Zhu R, Huang HH, Huang GL, Sun CT. Microstructure Continuum Modeling of an Elastic Metamaterial, *International Journal of Engineering Science* 49, 1477-1485, 2011.

[25] Zhou X, Hu G. Analytic Model of Elastic Metamaterials with Local Resonances, *Physical Review B* 79, 195109, 2009.

[26] Bigoni D, Guenneau S, Movchan AB, Brun M. Elastic Metamaterials with Inertial Locally Resonant Structures: Application to Lensing and Localization, *Phys. Rev. B* 87, 174303, 2013.

[27] Wu Y, Lai Y, Zhang ZQ. Elastic Metamaterials with Simultaneously Negative Effective Shear Modulus and Mass Density, *Physical Review Letters* 107, 105506, 2011.

[28] Grima JN, Caruana-Gauci R, Wojciechowski KW, Evans KE. Smart hexagonal truss systems exhibiting negative compressibility through constrained angle stretching, *Smart Mater. Structures* 22, 084015, 2013.

[29] Scarpa F, Tomlin PJ. On the transverse shear modulus of negative Poisson's ratio honeycomb structures Fatigue *Fract. Eng. Mater.* 23, 717–720, 2000.

[30] Lakes RS. Foam structures with a negative Poisson's ratio. *Science* 235, 1038–1040, 1987

[31] Nicolaou ZG, Motter AE. Mechanical Metamaterials with Negative Compressibility Transitions, *Nature Materials* 11, 608-613, 2012. Also: web-based Supplementary Information.

[32] Nicolaou ZG, Motter AE. Longitudinal Inverted Compressibility in Super-strained Metamaterials. *J Stat Phys* 151, 1162–1174, 2013.

[33] Chen ML, Karpov EG. Bistability and thermal coupling in elastic metamaterials with negative compressibility. *Physical Review E* 90, 033201, 2014.

[34] Chen ML, Karpov EK. Bistability and thermal coupling in elastic metamaterials with negative compressibility. Paper # 9429-50. *Bioinspiration, Biomimetics, and Bioreplication V, SPIE Smart Structures/NDE*, March 8-12, 2015, San Diego, CA.

[35] Hoff NJ. The applicability of Saint-Venant's principle to airplane structures. *Journal of Aeronautical Sciences* **12**, 455-460.

[36] Stephen NG, Wang PJ. On Saint-Venant's principle in pin-jointed frameworks. *International Journal of Solids and Structures* **33**(1), 79-97, 1996.

[37] Sadd MH. *Elasticity: Theory, Applications, and Numerics*, Elsevier, 2005

[38] Karpov EG, Stephen NG, Dorofeev DL. On Static Analysis of Finite Repetitive Structures by Discrete Fourier Transform. *International Journal of Solids and Structures* 39(16), 4291-4310, 2002.

[39] Karpov EG, Dorofeev DL, Stephen NG. Characteristic Solutions for the Statics of Repetitive Beam-Like Trusses. *International Journal of Mechanical Sciences* 44(7), 1363-1379, 2002.

[40] Liu WK, Karpov EG, Park HS. *Nano Mechanics and Materials: Theory, Multiscale Methods and Applications*. Wiley, 2006.

[41] Karpov EG, Park HS, Liu WK. A Phonon Heat Bath Approach for the Atomistic and Multiscale Simulation of Solids, *International Journal for Numerical Methods in Engineering* 70(3), 351–378, 2007.

[42] Karpov EG, Wagner GJ, Liu WK. A Green's Function Approach to Deriving Non-Reflecting Boundary Conditions in Molecular Dynamics Simulations, *International Journal for Numerical Methods in Engineering* 62(9), 1250-1262, 2005.

[43] Karpov EG, Yu H, Park HS, Liu WK, Wang JQ. Multiscale Boundary Conditions in Crystalline Solids: Theory and Application to Nanoindentation, *International Journal of Solids and Structures* 43(21), 6359–6379, 2006.

[44] Medyanik SN, Karpov EG, Liu WK. Domain Reduction Approach to Molecular Mechanics Simulations of Carbon Nanostructures, *Journal of Computational Physics* 218(2), 836–859, 2006.

[45] Qian D, Phadke M, Karpov EG. A Domain-Reduction Approach to Bridging-Scale Simulation of One-Dimensional Nanostructures, *Computational Mechanics* 47(1), 31-47, 2011.

[46] Schenk M, Guest SD. Geometry of Miura-Folded Metamaterials. *PNAS* 110(9), 3276–3281, 2013.

[47] Wei ZY, Guo ZV, Dudte L, Liang HY, Mahadevan L. Geometric Mechanics of Periodic Pleated Origami. *Physical Review Letters* 110, 215501, 2013.

[48] Silverberg JL, Evans AA, McLeod L, Hayward RC, Hull T, Santangelo CD, Cohen I. Using Origami Design Principles to Fold Reprogrammable Mechanical Metamaterials. *Science* 345, 647-650, 2014.

[49] Fleck NA, Qiu XM, The damage tolerance of elastic–brittle, two-dimensional isotropic lattices, *Journal of the Mechanics and Physics of Solids* 55 (2007) 562–588.

[50] Phani AS, Fleck NA, Elastic Boundary layers in two-dimensional isotropic lattices, *Journal of Applied Mechanics* 75 (2008) 021020.
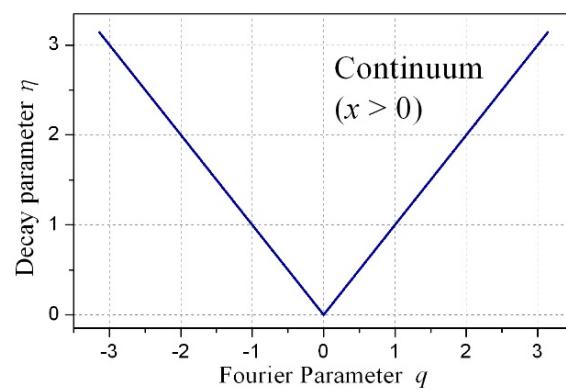
**Fig.1:** Deformation decay spectrum (the η-distribution) of the elastic continuum (1).
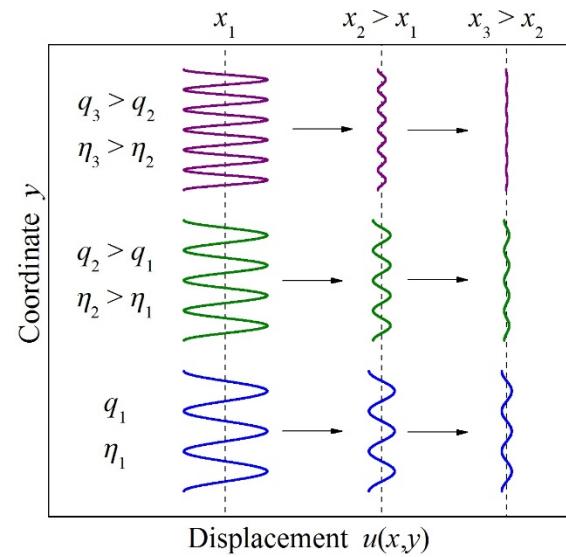
Fig.2: Compliance of Fourier mode solution for continua, Eq.(2), with the Saint-Venant end effect: finer modes (top) decay faster with x.
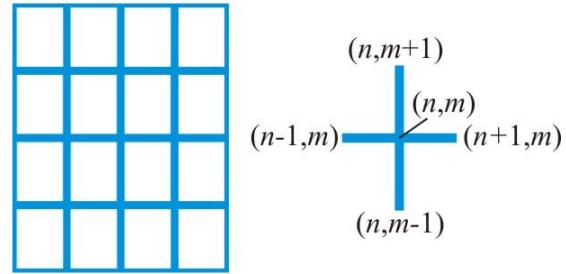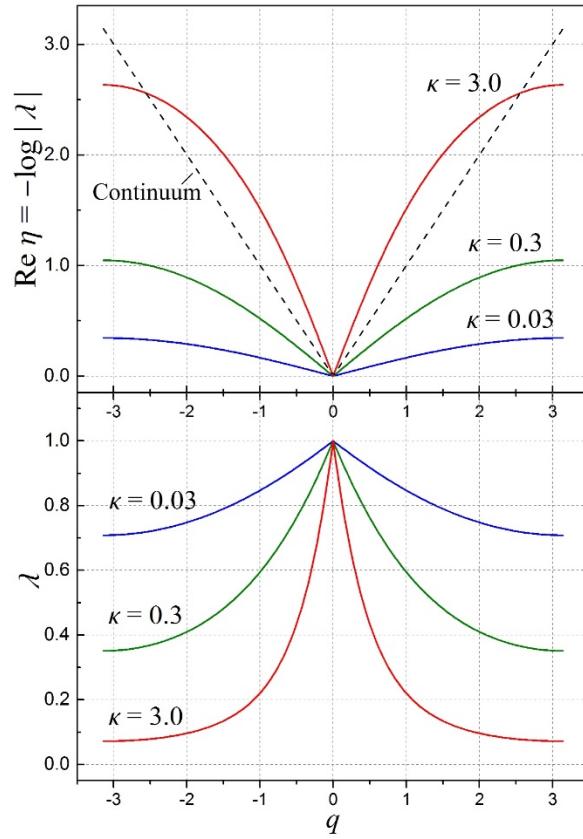
Fig.3: Rectangular grid structure: overall geometry and associate substructure; λ- and η-distributions for one DoF per node and various κ in (18).
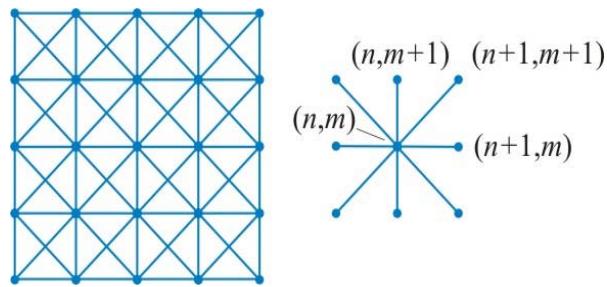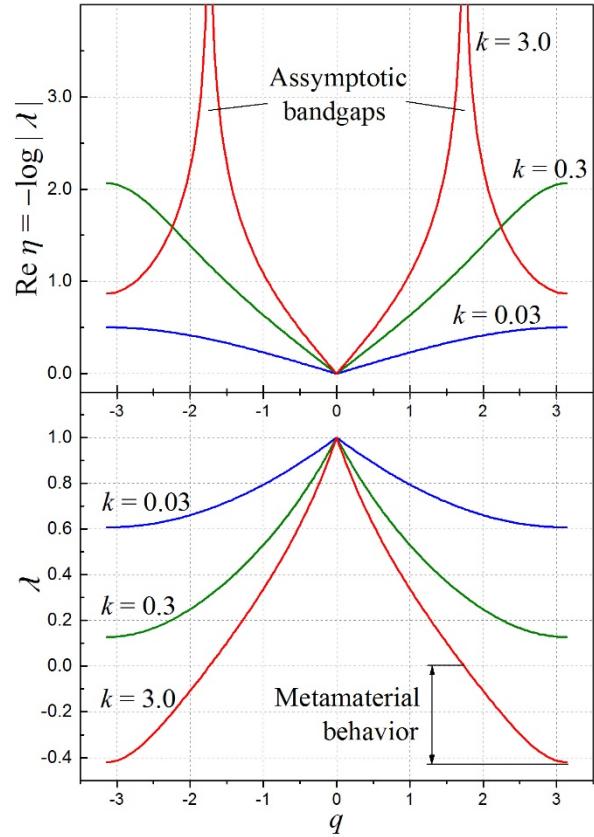
Fig.4: X-braced lattice with nonlocal diagonal interactions; λ-distribution with a negative zone and η-distribution with bandgaps at larger k in (20).
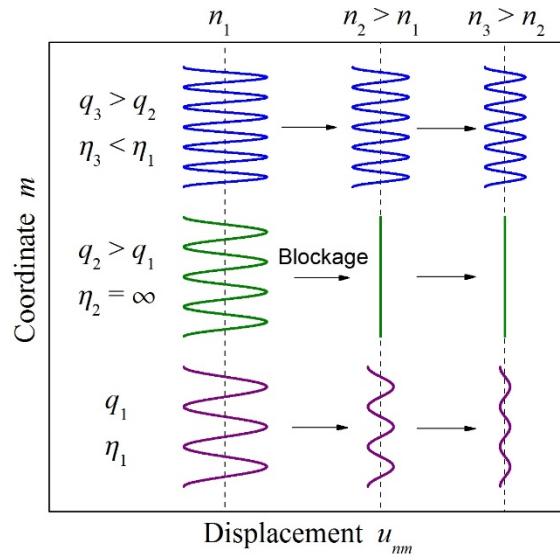
Fig.5: Reversal of the Saint-Venant edge effect in Fig.4 lattice: a denser Fourier mode propagates farer than a sparse one, and an intermediate mode can be completely blocked at the surface.
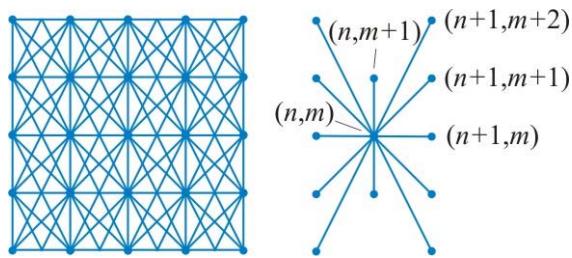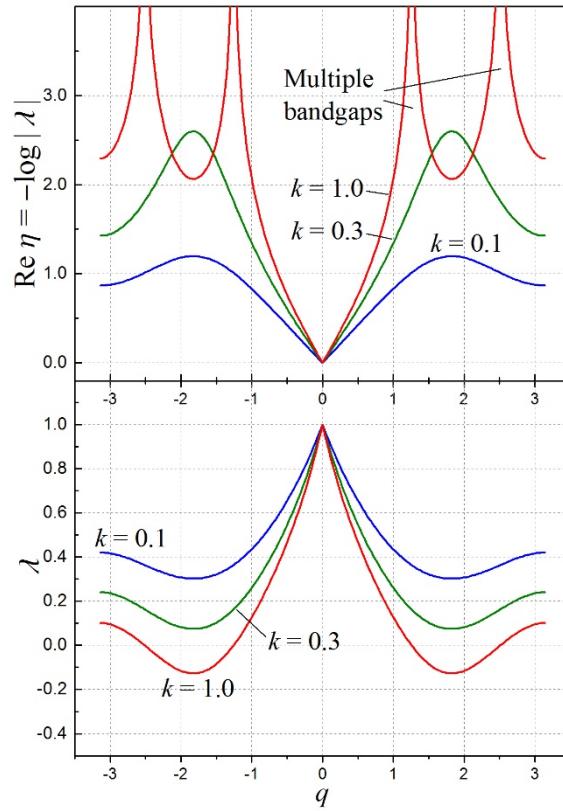
Fig.6: Latticework with farer-reaching direct interactions between nodes: overall geometry and associate substructure; λ-distribution entering the negative region and η-distribution showing multiple bandgaps at a larger value $k = k^{(1)} = k^{(2)}$ in equation (22).
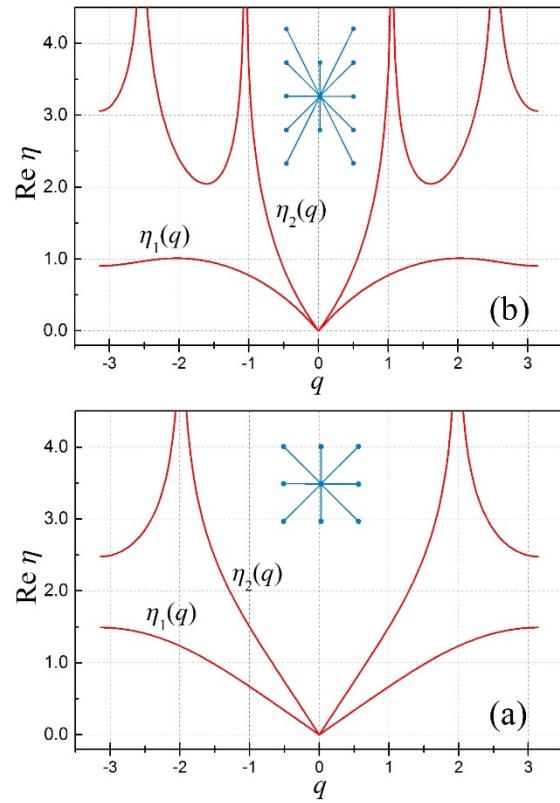
Fig.7: Examples of η-distribution behavior in lattices with two in-plane DoFs per node: (a) Fig.4 geometry, and (b) Fig.6 geometry.
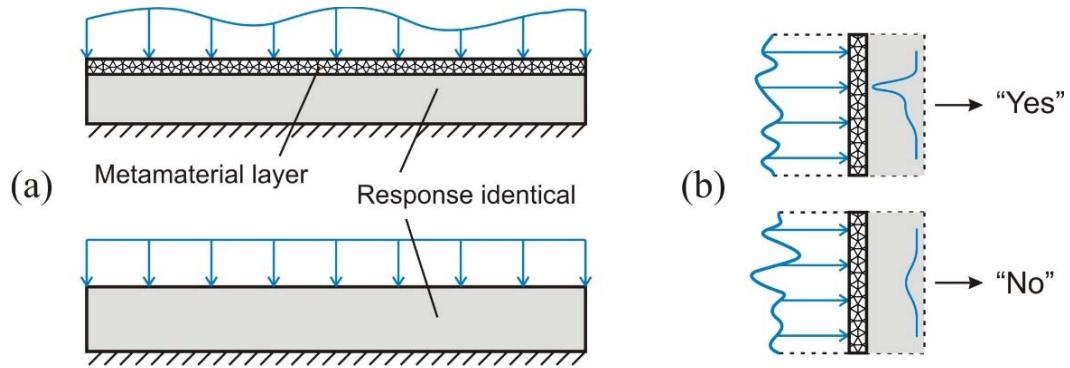
Fig.8: Concepts for the RSV metamaterials applications: (a) mitigation of surface pressure unevenness in structural blocks, and (b) *in situ* load pattern recognition.
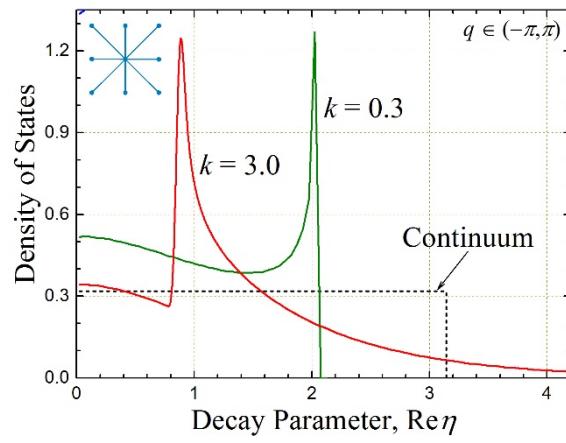
Fig.9: Density of states for the X-braced lattice of Fig.4 compared to an elastic continuum; a tail of fast decaying modes and a midrange peak are seen for the metamaterial at $k = 3.0$ in equation (17).
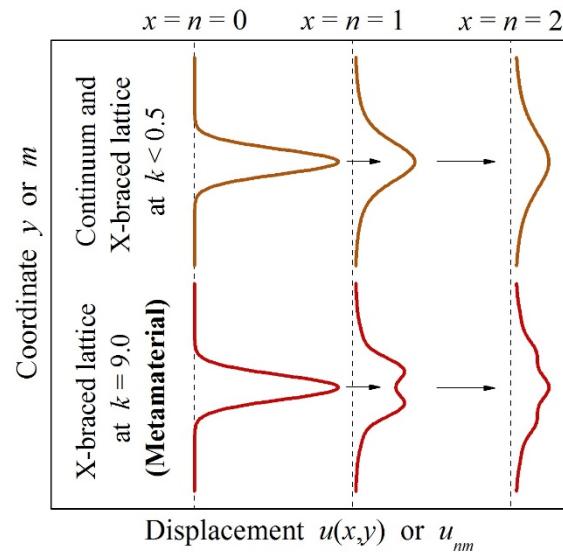
Fig.10: Dispersion of Gaussian deformation pattern by an X-braced lattice of Fig.4 at $k = 9.0$, compared to a continuum (1) and to itself at $k < 0.5$, where no dispersion occurs.
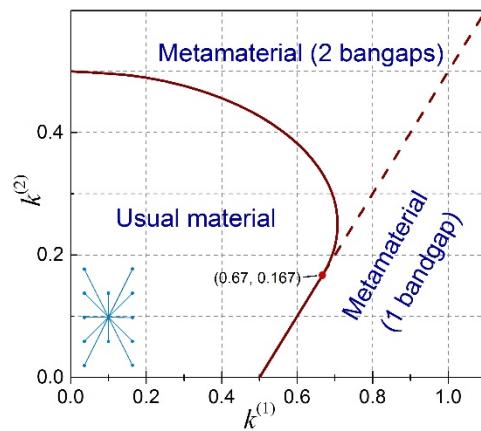
Fig.11: Phase diagram of Fig.6 lattice in terms of the structural parameters of equation (22).